

RADAR

Research Archive and Digital Asset Repository

OXFORD
BROOKES
UNIVERSITY

Cheung, C, Poolman, M, Fell, D, Ratcliffe, R and Sweetlove, L

A Diel Flux Balance Model Captures Interactions between Light and Dark Metabolism during Day-Night Cycles in C3 and Crassulacean Acid Metabolism Leaves

Cheung, C, Poolman, M, Fell, D, Ratcliffe, R and Sweetlove, L (2014) A Diel Flux Balance Model Captures Interactions between Light and Dark Metabolism during Day-Night Cycles in C3 and Crassulacean Acid Metabolism Leaves. *Plant Physiology*, 165 (2). pp. 917-929.

doi: [10.1104/pp.113.234468](https://doi.org/10.1104/pp.113.234468)

This version is available: <https://radar.brookes.ac.uk/radar/items/c7005009-4812-4918-9735-286b353cbdac/1/>

Available on RADAR: May 2016

Copyright © and Moral Rights are retained by the author(s) and/ or other copyright owners. A copy can be downloaded for personal non-commercial research or study, without prior permission or charge. This item cannot be reproduced or quoted extensively from without first obtaining permission in writing from the copyright holder(s). The content must not be changed in any way or sold commercially in any format or medium without the formal permission of the copyright holders.

This document is the postprint version of the journal article. Some differences between the published version and this version may remain and you are advised to consult the published version if you wish to cite from it.

1 **Running head:**

2

3 Integrated day-night model of leaf metabolism

4

5 **Corresponding authors:**

6

7 R.G. Ratcliffe and L.J. Sweetlove*

8 Department of Plant Sciences,

9 University of Oxford,

10 South Parks Road,

11 Oxford OX1 3RB

12 U.K.

13

14 +44 1865 275000

15 george.ratcliffe@plants.ox.ac.uk

16 lee.sweetlove@plants.ox.ac.uk

17

18 *For editorial correspondence and proofs

19

20 **Journal area:**

21

22 Systems and Synthetic Biology

23 **A diel flux-balance model captures interactions between light and**
24 **dark metabolism during day-night cycles in C₃ and CAM leaves.**

25

26 C.Y. Maurice Cheung¹, Mark G. Poolman², David. A. Fell², R. George Ratcliffe¹ and
27 Lee J. Sweetlove¹

28

29 ¹ Department of Plant Sciences, University of Oxford, South Parks Road, Oxford,
30 OX1 3RB, UK

31 ² School of Life Sciences, Oxford Brookes University, Headington, Oxford OX3 0BP,
32 UK

33

34 **One sentence summary:**

35 A diel flux balance modeling framework that integrates temporally-separated metabolic
36 networks provides realistic descriptions of light and dark metabolism in C₃ and CAM leaves,
37 and suggests that energetics and nitrogen use efficiency are unlikely to have been drivers
38 for the evolution of CAM.

39 **Funding:**

40

41 CYMC was supported by a studentship from the University of Oxford Systems
42 Biology Doctoral Training Centre funded by the Clarendon Fund and a Sloane-
43 Robinson award from Keble College, Oxford.

44

45 **Corresponding authors:**

46

47 R. George Ratcliffe, george.ratcliffe@plants.ox.ac.uk

48 * Lee J. Sweetlove, lee.sweetlove@plants.ox.ac.uk

49

50 * For editorial correspondence and proofs

51

52 **ABSTRACT**

53 Although leaves have to accommodate markedly different metabolic flux patterns in
54 the light and the dark, models of leaf metabolism based on flux balance analysis
55 (FBA) have so far been confined to consideration of the network under continuous
56 light. A new FBA framework is presented that solves the two phases of the diel cycle
57 as a single optimisation problem and thus provides a more representative model of
58 leaf metabolism. The requirement to support continued export of sugar and amino
59 acids from the leaf during the night, as well as to meet night-time cellular
60 maintenance costs, forces the model to set aside stores of both carbon and nitrogen
61 during the day. With only minimal constraints, the model successfully captures many
62 of the known features of C₃ leaf metabolism, including the recently discovered role of
63 citrate synthesis and accumulation in the night as a precursor for the provision of
64 carbon skeletons for amino acid synthesis during the day. The diel FBA model can
65 be applied to other temporal separations such as that which occurs in CAM
66 photosynthesis, allowing a system-level analysis of the energetics of CAM. The diel

67 model predicts that there is no overall energetic advantage to CAM, despite the
68 potential for suppression of photorespiration through CO₂ concentration. Moreover,
69 any savings in enzyme machinery costs through suppression of photorespiration are
70 likely to be offset by the higher flux demand of the CAM cycle. It is concluded that
71 energetic or nitrogen-use considerations are unlikely to be evolutionary drivers for
72 CAM photosynthesis.

73

74 INTRODUCTION

75 Photosynthetic metabolism continues to be studied intensively due to its
76 importance for crop performance and for the global carbon cycle in relation to climate
77 change. The metabolic pathways and enzymes involved in carbon fixation and
78 related metabolic processes such as the synthesis of sucrose and starch have been
79 well characterised. However, it is apparent that a full appreciation of leaf metabolism
80 requires these metabolic processes to be placed in the context of the wider
81 metabolic network ([Szecowka et al., 2013](#)). This is particularly important for
82 predicting how strategies for engineering improved photosynthesis ([Maurino and](#)
83 [Weber, 2013](#)) may affect network properties such as redox and energy balancing
84 ([Kramer and Evans, 2011](#)).

85 Flux-balance analysis has emerged as the method of choice for predicting
86 fluxes in large metabolic network models ([Sweetlove and Ratcliffe, 2011](#)) and
87 several flux-balance models have explicitly considered photosynthetic metabolism in
88 a variety of plants species and microorganisms. These include cyanobacteria ([Knoop](#)
89 [et al., 2010](#); [Montagud et al., 2010](#); [Nogales et al., 2012](#); [Saha et al., 2012](#); [Knoop et](#)
90 [al., 2013](#)), Chlamydomonas ([Boyle and Morgan, 2009](#); de Oliveira [Dal'Molin et al.,](#)
91 [2011](#)), Arabidopsis ([de Oliveira Dal'Molin et al., 2010a](#)), rapeseed embryos ([Hay and](#)
92 [Schwender, 2011](#)), rice ([Poolman et al., 2013](#)), maize ([Saha et al., 2011](#)) and several
93 C₄ plants ([de Oliveira Dal'Molin et al., 2010b](#)). These models successfully predicted
94 the metabolic routes involved in the fixation of CO₂ into different biomass
95 components in the light. However, one major feature of metabolism of photosynthetic
96 organisms, namely the interactions between light and dark metabolism is neglected
97 in most of these studies. Effectively, most models assume that the organism grows
98 in constant light which is rarely true in natural conditions.

99 Apart from the obvious switch from photoautotrophic to heterotrophic
100 metabolism between day and night, interactions between the two phases can occur
101 through the temporal separation of storage compound synthesis and subsequent
102 mobilisation. For example, it has been shown that the carbon skeletons used for
103 nitrogen assimilation during the day are largely provided by carboxylic acids that
104 were synthesised and stored during the previous night ([Gauthier et al., 2010](#)). Such
105 temporal shifts of carbon and nitrogen metabolism have substantial implications for
106 fluxes in the central metabolic network of leaves in the light ([Tcherkez et al., 2009](#)).
107 Interactions between temporally separated metabolic events are also a critical

108 feature of crassulacean acid metabolism (CAM) photosynthesis in which CO₂ is
109 initially fixed at night via PEP carboxylase, leading to night-storage of carboxylic
110 acids (mainly malic acid) which are decarboxylated during the day to provide CO₂ for
111 the conventional photosynthetic carbon assimilation cycle. While this is principally an
112 adaptation to arid environments, there are unresolved questions as to whether CAM
113 photosynthesis is energetically more efficient than C₃ photosynthesis ([Winter and
114 Smith, 1996](#)). Such questions are becoming more important in the light of the
115 proposed use of CAM plants as a source of biofuel ([Yan et al., 2011](#)).

116 One recent study has used flux-balance analysis to consider both light and
117 dark metabolism in *Synechocystis* over a complete diel cycle divided into 192 time
118 steps ([Knoop et al., 2013](#)). Time-courses of metabolic flux predictions over a diel
119 cycle were simulated by altering the constraints on metabolic outputs (biomass
120 composition) depending on the time-point and based on empirical rules. This led to a
121 highly constrained model and did not allow the range of potential interactions
122 between the day and night phases to be fully explored. We have developed an
123 alternative modelling framework for integrated day-night flux-balance analysis in
124 which the metabolic fluxes in the light phase and the dark phase were simulated
125 simultaneously in a single optimisation problem. A pre-defined list of storage
126 compounds that can accumulate freely over the diurnal cycle was made available to
127 the model. The model was then free to choose amongst these storage compounds,
128 the choice being dictated by the need to satisfy the objective function within the
129 applied constraints. This diurnal modelling framework was used to explore the
130 interactions between light and dark metabolism and to predict the metabolic fluxes in
131 the light in both C₃ and CAM photosynthesis. We show that accounting for day-night
132 interactions leads to an altered pattern of fluxes during the day that provides a better
133 match with experimental observations. We were also able to simulate network flux
134 distributions in CAM metabolism. The model successfully predicts the classical CAM
135 cycle in the different CAM subtypes and allows a comparison of the energetic
136 efficiency and metabolic costs between CAM and C₃ photosynthetic metabolism.

137

138 **RESULTS**

139

140 **A day-night modelling framework for leaf metabolism**

141

142 The aim was to construct a flux-balance model that accounted for the day and
143 night phases of leaf metabolism in an integrated fashion such that storage
144 compounds synthesised during the day were available for use in the dark and vice
145 versa. This was achieved by applying a specific framework of constraints to an
146 existing genome-scale model of Arabidopsis metabolism ([Cheung et al., 2013](#)). The
147 assumption was made that each phase (day and night) was in a pseudo-steady-
148 state, as has been done for previous flux-balance models of photosynthetic
149 metabolism. The two inter-dependent steady states were modelled as a single
150 optimisation problem with photoautotrophic metabolism specified in the day by
151 allowing a photon influx, and heterotrophic metabolism specified at night by setting
152 the photon influx to zero. For simplicity a 12 h-12 h day-night cycle was specified.
153 Also for simplicity, we considered the case of a mature leaf in which the only
154 metabolic outputs were the synthesis of sucrose and a range of amino acids for
155 export to the phloem. It is trivial to extend the model to consider a growing leaf and
156 to account for shorter or longer days.

157 The relative proportions of 18 amino acids exported to the phloem
158 (Supplemental Table 1) and the ratio of sucrose to total amino acid export (2.2:1)
159 were constrained in accordance with measurements of the composition of
160 Arabidopsis phloem exudate (Wilkinson and Douglas, 2003). The model was
161 required to maintain export of sugars and amino acids to the phloem during the day
162 and night, but at a ratio of 3:1 (day: night) based on measurements in Arabidopsis
163 rosettes ([Gibon et al., 2004](#)). The sole source of nitrogen for the leaf model was
164 nitrate import from the xylem, based on the observation that nitrate represents the
165 main form of nitrogen (80%) entering a leaf (Macduff and Bakken, 2003). The rate of
166 nitrate import into the leaf during the day and the night was constrained to be 3:2
167 based on measurements in various plant species ([Delhon et al., 1995](#); [Macduff and
168 Bakken, 2003](#); [Siebrecht et al., 2003](#)). Besides the export of sucrose and amino-
169 acids, cellular maintenance costs were accounted for by including generic ATPase
170 and NADPH oxidase steps for maintenance and the requirement to satisfy a
171 specified carbon conversion efficiency (Cheung et al., 2013). In this case, we
172 assumed a carbon conversion efficiency of 50% during the night based on the day-
173 night carbon balance calculated from measurements in Arabidopsis rosettes ([Gibon
174 et al., 2004](#)). The ratio of ATP maintenance cost to NADPH maintenance cost was
175 assumed to be 3:1 ([Cheung et al., 2013](#)) and maintenance costs were assumed to

176 be the same in the light and dark phases. In addition to the above constraints, fluxes
177 through the chloroplastic NADPH dehydrogenase (NDH) and plastoquinol oxidase
178 were set to zero as the contributions of NDH ([Yamamoto et al., 2011](#)) and
179 plastoquinol oxidase ([Josse et al., 2000](#)) to photosynthesis are thought to be minor.
180 The flux of sucrose synthase was constrained to be irreversible in the direction of
181 sucrose degradation, as it is thought that sucrose synthase is not involved in sucrose
182 synthesis in leaves ([Nguyen-Quoc et al., 1990](#)).

183 In order to maintain a metabolic output at night, the model must accumulate
184 carbon and nitrogen stores during the day. To explore the metabolic interaction
185 between the day and the night, the model included a set of sugars and carboxylic
186 acids to be utilised as carbon storage molecules. Specifically, starch, glucose,
187 fructose, malate, fumarate and citrate were free to accumulate during either the day
188 or night phase. No direct constraints were applied to the amount of each compound
189 that accumulated other than the requirement for the overall model to be mass
190 balanced. For nitrogen, nitrate and the 20 common amino acids were allowed to
191 accumulate as storage compounds, but the latter were constrained such that
192 accumulation was only permitted during the day but not at night, in accordance with
193 observations on the diel fluctuations of amino-acids in leaves ([Scheible et al., 2000](#)).
194 Again, no direct constraints were applied to the amount of each amino acid to be
195 accumulated. Thus the model was free to choose among a set of storage
196 compounds to allow the constraint of export of sugars and amino acids at night to be
197 met. The interconnections between the light and dark phases of the model, as well
198 as the input and output constraints, are summarised in Fig. 1. Fluxes were predicted
199 using linear programming with an objective function to minimise the sum of fluxes
200 within the specified constraints. The two phases were modelled simultaneously in a
201 single optimisation problem analogous to modelling interactions between two micro-
202 organisms or two tissues/cell-types in multicellular organisms ([de Oliveira Dal'Molin
203 et al., 2010b](#)). As Arabidopsis is a C₃ plant, the ratio of Rubisco carboxylation to
204 oxygenase was set to a typical value of 3:1 to simulate photorespiration (Gutteridge
205 and Pierce, 2006).

206

207 **The integrated day-night model leads to altered flux predictions in comparison**
208 **to a constant light model**

209

210 To assess the effect of the diel modelling framework, fluxes predicted in the
211 light phase of the diel model were compared to those predicted in a constant-light
212 model. The latter model was constrained by total sucrose and amino-acid export and
213 cellular maintenance costs that matched those over a 24-hour period in the diel
214 model.

215 To take account of the fact that some fluxes are not uniquely defined at the
216 optimum, flux variability analysis was used to determine the feasible range of all
217 fluxes. Fluxes in the light component of the diel model were considered to be
218 significantly different from those of the same reactions in the constant light models if
219 their flux ranges did not overlap. This procedure identified 131 reactions with non-
220 overlapping flux ranges in the light (Supplemental Table II). These reactions carried
221 different fluxes in the light, but none carried flux in opposite directions in the two
222 models. Fluxes were compared using a similarity measure calculated from the
223 fraction of the smaller flux value over the larger flux value. Reactions with a similarity
224 measure of less than 0.25 are listed in Table I, where the smaller the value of this
225 measure, the larger the difference in fluxes. A similarity measure of zero means that
226 the reaction carried zero flux in one of the models. Some reactions that carried
227 different fluxes between the diel and constant light models are to be expected. For
228 example, starch synthesis was turned on during the day in the diel model, but not in
229 the constant light model where there was no need to store carbon because of the
230 continuous assimilation of CO₂. Similarly transport of carboxylic acids and nitrate
231 across the tonoplast for storage in the vacuole was activated in the diel model.

232 However, there were also changes in metabolic fluxes that were less directly
233 constrained. These relate to the citrate used to provide carbon skeletons for
234 glutamate and glutamine synthesis in the light. Table I shows that the synthesis of
235 citrate was predicted to occur in the peroxisome via peroxisomal citrate synthase. In
236 contrast, the diel model predicted that citrate would be synthesised via the
237 mitochondrial TCA cycle during the night and stored in the vacuole. Nocturnally
238 stored citrate was then exported from the vacuole during the day and metabolised
239 into 2-oxoglutarate via aconitase and isocitrate dehydrogenase for glutamate
240 synthesis (Fig. 2). The prediction of the diel model is consistent with observations
241 from isotopic labelling experiments ([Gauthier et al., 2010](#)) and this example
242 demonstrates the importance of considering the interconnections between light and
243 dark metabolism for the prediction of realistic flux distributions.

244

245 **Predictions of metabolic network fluxes in a mature C₃ leaf over a day-night**
246 **cycle**

247

248 The flux solution using the day-night modelling framework can be summarised
249 in a simple flux map (Fig. 3) and a complete list of predicted flux ranges for reactions
250 in the light and dark are provided in Supplemental Table III. The diurnal modelling
251 framework successfully predicted that starch is the main carbon storage compound
252 that accumulates in the light even though the model was free to utilise sugars and
253 carboxylic acids as the carbon store. Some malate was also predicted to accumulate
254 in the light, which then fed into the TCA cycle in the dark. Interestingly, the model
255 predicted that both citrate and nitrate were stored at night in order to support
256 nitrogen assimilation which was predicted to occur primarily during the day. The
257 nitrate store was generated by transporting imported nitrate from the xylem into the
258 vacuole during the night and release of the vacuolar store to the cytosol during the
259 day. The model also predicted the storage during the day of a proportion of amino
260 acids synthesised in the light and these were then exported into the phloem in the
261 dark.

262 In the light phase, the model predicted large fluxes through the linear
263 photosynthetic electron transport pathway and the Calvin-Benson pathway to
264 support sucrose and amino acid synthesis and starch accumulation. The classical
265 photorespiratory pathway for the oxidation of 2-phosphoglycolate was also predicted
266 to be active due to a constraint in the model that set the Rubisco carboxylation to
267 oxygenase ratio to 3:1. Note, that if this constraint is removed, the Rubisco
268 oxygenase reaction become inactive. The TCA cycle was predicted to operate in a
269 non-cyclic mode in the light with two separate branches (Fig. 4) consistent with the
270 current understanding based on isotope labelling experiments, and as predicted from
271 other flux-balance models ([Sweetlove et al., 2010](#)). Oxaloacetate produced from
272 phosphoenolpyruvate carboxylase was converted into malate which accumulated in
273 the light. The model predicted that the mitochondrial electron transport chain (ETC)
274 is active in the light, carrying a flux equivalent to 10% of the flux through
275 photosynthetic linear electron transport. The mitochondrial ATP synthase was
276 predicted to contribute to 18% of total ATP synthesis in the light with the rest
277 produced by the chloroplast thylakoid ATP synthase. The two sources of NADH

278 feeding into the mitochondrial ETC are glycine decarboxylase and the malate-
279 oxaloacetate shuttle (Fig. 5) with contributions of 53% and 47% respectively (the
280 mitochondrial isocitrate dehydrogenase reaction is predicted to exclusively generate
281 NADPH which is used for maintenance reactions in the mitochondrion). The ultimate
282 source of reductant in a photosynthetic leaf is from the photosynthetic linear electron
283 transport. While most of the reducing power is used for photosynthetic CO₂ fixation
284 in the chloroplast, a small proportion of reductant was shuttled out of the chloroplast
285 by the malate-OAA shuttle (11%) and the 3-phosphoglycerate (3PGA)-
286 glyceraldehyde 3-phosphate (GAP) shuttle (4%) (Fig. 5). Malate-OAA exchanges
287 were responsible for transfer of reductant from the chloroplast into the cytosol, the
288 mitochondrion and the peroxisome. The 3PGA-GAP shuttle transported reductant
289 from the chloroplast to the cytosol to produce NADPH by the non-phosphorylating
290 NADP-GAPDH. A proportion of NADPH produced in the cytosol was shuttled into the
291 mitochondrion by the isocitrate-2-oxoglutarate shuttle (Fig. 5).

292 In the dark phase, the largest fluxes are related to starch degradation,
293 sucrose synthesis, glycolysis, the oxidative pentose phosphate pathway (OPPP), the
294 TCA cycle and the mitochondrial electron transport chain (Fig. 3). The breakdown of
295 starch was predicted to be carried out by the hydrolytic pathway generating maltose
296 for transport from the chloroplast to the cytosol. This is the result of constraining the
297 chloroplastic hexose phosphate transporter to carry zero flux, in line with
298 experimental observations ([Niewiadomski et al., 2005](#)), thus limiting the possible
299 metabolic routes for carbon export from the chloroplast. When this constraint was
300 removed starch breakdown occurred via starch phosphorylase. Glycolysis and the
301 OPPP were predicted to occur in both the cytosol and the chloroplast, with 72% of
302 the total flux through glycolytic glyceraldehyde 3-phosphate dehydrogenase and
303 55% of that through the OPPP glucose 6-phosphate dehydrogenase steps occurring
304 in the cytosol. The TCA cycle operates in a cyclic mode in the dark (Fig. 4)
305 consuming pyruvate produced from stored starch via glycolysis. A small proportion of
306 the citrate produced by citrate synthase (15%) is stored in the dark to provide carbon
307 skeletons for glutamate and glutamine synthesis in the light.

308

309 **Predictions of metabolic fluxes in a mature CAM leaf over a diurnal cycle**

310

311 From a structural metabolic modelling perspective, the Arabidopsis genome-
312 scale metabolic model contains all the metabolic reactions required to carry out the
313 various subtypes of CAM photosynthesis. However, because the metabolic cycle
314 that constitutes CAM photosynthesis is temporally segregated, metabolism in CAM
315 leaves cannot be modelled with a single-steady state FBA model. We therefore
316 applied the diel modelling framework to predict metabolic fluxes in a mature CAM
317 leaf over a 24-hour cycle. As for the mature C₃ leaf, the model was constrained by
318 sucrose and amino acid export and cellular maintenance costs. The main additional
319 constraint for simulating CAM photosynthesis was that CO₂ exchange with the
320 environment was set to have zero flux in the light to simulate the closure of stomata
321 in CAM plants during the day. Other differences between the C₃ and CAM models
322 arose from the treatment of the Rubisco oxygenase activity and the export of carbon
323 from the plastids. First, Rubisco oxygenase activity is likely to be suppressed in CAM
324 leaves in the light due to the increase in the internal partial pressure of CO₂, but
325 since there is also an increase in internal oxygen concentration, it is unclear to what
326 extent photorespiration is prevented in CAM plants ([Lüttge, 2011](#)). Accordingly the
327 Rubisco carboxylase to oxygenase ratio was left unconstrained in the light phase of
328 the CAM model. Secondly, in the ice plant *Mesembryanthemum crystallinum* L., a
329 facultative CAM plant, chloroplasts of CAM-induced plants mainly export glucose 6-
330 phosphate ([Neuhaus and Schulte, 1996](#)) and this is coincident with a 71-fold
331 increase in transcript level for the chloroplastic G6P transporter ([Cushman et al.,
332 2008](#)). On this basis, the chloroplastic glucose 6-phosphate transporter was not
333 constrained in the CAM model. Finally the various subtypes of CAM photosynthesis
334 were simulated by setting the reactions specific to other subtypes to carry zero flux.
335 The constraints applied for modelling the different modes of photosynthesis are
336 summarised in Table II.

337 Using the diel modelling framework with CAM-specific constraints, FBA
338 successfully predicted metabolic fluxes consistent with the well-known CAM cycle
339 (Supplemental Table III). In the light, nocturnally stored malate was decarboxylated
340 by malic enzyme or PEPCK depending on the subtype. In the generic CAM model
341 (no sub-type constraints), 89% of malate decarboxylation was predicted to be carried
342 out by PEPCK, with the remaining 11% carried out by the cytosolic malic enzyme. In
343 addition to the photosynthetic linear electron transport and reductive pentose
344 phosphate pathway, which were expected to carry high fluxes in the light, the

345 gluconeogenesis pathway also carried a high predicted flux in the light to convert
346 PEP, from malate decarboxylation, to starch or soluble sugars for storage as part of
347 the CAM cycle. In the generic CAM model, only starch was stored during the day but
348 not soluble sugars. In our initial models of the sugar-storing subtypes, fructose was
349 produced in the cytosol by sucrose synthase and subsequently transported into the
350 vacuole by the vacuolar hexose transporter. However, it is thought that tonoplast
351 hexose transport activity is restricted to the night (in an efflux capacity) in CAM
352 plants to avoid futile cycling ([Holtum et al., 2005](#); [Antony et al., 2008](#)). When the
353 vacuolar hexose transporter activity was subsequently restricted to the dark period,
354 the model predicted that sucrose is imported into the vacuole and catabolised into
355 glucose and fructose by vacuolar invertase, which is in line with postulated models in
356 the literature ([Smith and Bryce, 1992](#); [McRae et al., 2002](#); [Holtum et al., 2005](#)).

357 The Rubisco carboxylase to oxygenase ratio was unconstrained in modelling
358 CAM and the model predicted no Rubisco oxygenase flux suggesting that Rubisco
359 oxygenase is not necessary for the functioning of a mature CAM leaf under the
360 assumption of minimising total flux. The mitochondrial ETC and ATP synthase
361 carried high fluxes in the light with the mitochondrial ETC carrying a flux equivalent
362 to 29% of the flux through photosynthetic linear electron transport and the
363 mitochondrial ATP synthase contributing to 34% of the total ATP produced in the
364 light in the generic CAM model. Similar values were predicted for the various CAM
365 subtypes. Similar to C₃ leaves, an incomplete TCA cycle was predicted in the light
366 phase with two separate branches, citrate to 2-oxoglutarate and succinate to
367 oxaloacetate (Fig. 6). Interestingly, the oxaloacetate-branch differed from that found
368 for the C₃ model in that oxaloacetate was produced, not consumed and succinate
369 was the starting point of the branch, not fumarate (Figs. 4 and 6). In the CAM TCA
370 cycle, the two branches are joined via the activity of isocitrate lyase in the
371 peroxisome to produce succinate (Fig. 6).

372 In the dark phase, the stored carbon (starch or soluble sugars) was predicted
373 to be catabolised to produce PEP, the substrate for carboxylation, via glycolysis.
374 PEP was carboxylated by PEP carboxylase to produce oxaloacetate, which was
375 subsequently converted into malate for storage in the vacuole as malic acid during
376 the night. With respect to starch degradation, the phosphorolytic route via starch
377 phosphorylase was predicted in CAM because it is more energetically efficient than
378 the hydrolytic route via maltose, and this is consistent with the current view of the

379 CAM cycle ([Weise et al., 2011](#)). While most of the carbon store was used to provide
380 the substrate for carboxylation in the CAM cycle, some went into the OPPP, to
381 produce NADPH for maintenance processes, and into the TCA cycle, to produce
382 NADH for ATP synthesis via the mitochondrial ETC and ATP synthase. As in a
383 mature C₃ leaf, the model predicted a complete TCA cycle in the dark in a mature
384 CAM leaf (Fig. 6).

385

386 **Quantitative comparisons of metabolism between C₃ and CAM leaves**

387

388 The CO₂-concentrating mechanism in CAM is an energy-requiring process
389 and the energetic cost of supporting sucrose and amino acid export from mature
390 leaves and cell maintenance processes was compared between C₃ and CAM in
391 terms of photon use (Fig. 7). Photon use in a mature CAM leaf is similar to that in a
392 C₃ leaf, being ±10% of C₃ depending on the CAM subtype.

393 Rubisco is the most abundant protein on earth, contributing up to 50% of the
394 soluble protein and 20-30% of the total nitrogen in a C₃ leaf (Feller et al., 2008). The
395 investment in Rubisco, in terms of energy and nitrogen, is likely to contribute
396 significantly to the evolutionary fitness trade-off in plants. By comparing the model
397 predictions, it was apparent that total flux through Rubisco (carboxylase + oxygenase
398 flux) was lower in CAM than C₃, mainly as a consequence of the prediction of no
399 oxygenase activity in the CAM model (Fig. 7). While this may suggest a cost-saving
400 for a CAM plant, it is offset by the fact that the CO₂-concentrating mechanism
401 requires high fluxes through the CAM cycle. As a consequence, the total flux through
402 the entire metabolic network is 32-64% higher in CAM than in C₃ (Fig. 7).

403

404 **DISCUSSION**

405

406 **Integration of light and dark metabolism is required to capture known features 407 of leaf metabolism by FBA**

408

409 The usefulness of constraints-based modelling tools such as FBA depends on
410 the extent to which they capture known features of the metabolic network. Good
411 agreement has been reported between the predicted and measured fluxes for a
412 heterotrophic Arabidopsis cell culture, leading to insights into cell maintenance costs

413 under stress conditions (Cheung et al., 2013). There is an expectation that a similar
414 modelling approach will be useful in analysing photosynthetic metabolism, but most
415 applications to date have been based on the analysis of the network under
416 conditions of constant light. Here analysis of the Arabidopsis model revealed that
417 there are several features of leaf metabolism that can only be captured by FBA by
418 considering the interaction between the temporally-separated phases of light and
419 dark metabolism. For example, the diel model accumulated citrate in the vacuole
420 during the night and this was released during the day to provide carbon skeletons for
421 nitrogen assimilation. This agrees with evidence from isotope labelling experiments
422 ([Gauthier et al., 2010](#)) and the current view of carboxylic acid metabolism in leaves
423 in the light (Tcherkez et al., 2009; [Sweetlove et al., 2010](#)). In contrast, a single-
424 steady-state, constant light FBA leaf model generated citrate via an unusual
425 metabolic route involving threonine aldolase and peroxisomal citrate synthase. This
426 route is most likely chosen by the model because of its efficiency in terms of carbon
427 use: the route leads to the fixation of 1 CO₂ by PEP carboxylase and releases 0.5
428 CO₂ from the recycling of glycine via the photorepiratory pathway. In another
429 Arabidopsis genome-scale metabolic model, the threonine aldolase reaction was
430 absent and the model predicted that citrate would be synthesised from pyruvate by
431 pyruvate dehydrogenase and mitochondrial citrate synthase ([de Oliveira Dal'Molin et
432 al., 2010a](#)), contradicting well-established evidence that the mitochondrial pyruvate
433 dehydrogenase is inhibited transcriptionally and post-transcriptionally in leaves in the
434 light ([Tovar-Mendez et al., 2003](#)).

435 A possible explanation for the accumulation of citrate in the dark over the
436 synthesis of citrate from primary photosynthate in the light could be that the
437 degradation of starch to produce citrate (via glycolysis, PEP carboxylase, pyruvate
438 dehydrogenase and citrate synthase) provides a carbon-neutral route for transferring
439 ATP and reducing power from the light phase to the dark phase. This conserves the
440 net carbon required to support dark metabolism, where citrate in the dark would
441 otherwise be metabolised through the TCA cycle and the carbon would be released
442 as CO₂. Confirming this, if the model was configured with citrate accumulation
443 prevented, the total CO₂ release in the dark was increased by 2%.

444 The diel model was free to choose between a range of carbon- (starch,
445 sugars and carboxylic acids) and nitrogen-storage compounds (nitrate and amino
446 acids) to support the export of sugars and amino acids during the night, and to meet

447 the night-time maintenance costs. The fact that the model solution selected starch
448 and amino acids as the main daytime storage carbon and nitrogen compounds,
449 respectively, consistent with the known biochemistry of C₃ leaves, reflects the
450 success of the objective function (minimisation of sum of fluxes) in capturing the
451 drivers that shape the metabolic system. Essentially, the choice of starch over
452 sugars and amino acids over nitrate storage, leads to a more efficient metabolic
453 network. For example, it is energetically less costly to mobilise a plastidic starch
454 store than a vacuolar sucrose store. Leaf starch breakdown initially occurs
455 hydrolytically in the plastid to generate maltose which is then metabolised to hexose
456 phosphate by a combination of the cytosolic enzymes glucosyltransferase,
457 hexokinase and α -glucan phosphorylase (Zeeman et al., 2004). The latter enzyme
458 uses Pi rather than ATP as the phosphoryl donor, and hence saves an ATP
459 compared to the breakdown of vacuolar sucrose via invertase and phosphorylation
460 by hexokinases. The choice of starch over carboxylic acids is again driven by the
461 efficiency driver of the objective function: carboxylic acids are more oxidised than
462 starch and hence the energy stored per carbon is less than for starch. The model
463 also correctly predicted that nitrate assimilation would occur only during the day, it
464 being overall more efficient (lower sum of fluxes) to store nitrate that is imported into
465 the leaf at night and release it from the vacuole (along with appropriate quantities of
466 citrate) during the day for assimilation into amino acids, consistent with experimental
467 measurements ([Stitt et al., 2002](#)).

468 However, it should be noted that the behaviour of all these models is highly
469 dependent on the accuracy of the reaction list and the nature of the constraints
470 applied. The choice of objective function will also affect the flux solution, although we
471 have previously demonstrated that the choice of objective function is less important
472 than the constraints applied to an FBA model of heterotrophic metabolism (Cheung
473 et al., 2013). Similarly, for this model, the use of other objective functions (e.g.
474 minimisation of photon use) did not change the main conclusions about the operation
475 of the network through the diel cycle. Having established that the diel modelling
476 framework can capture realistic aspects of leaf metabolism through the day-night
477 cycle, it can be employed in future to examine how the predicted flux distribution
478 changes in response to different metabolic scenarios such as variations in available
479 light for photosynthesis and the transition from sink to source leaves.

480

481 **The diel metabolic modelling framework allows simulation and analysis of**
482 **CAM**

483

484 The diel framework for FBA also allows CAM photosynthesis to be tackled for
485 the first time. Only minimal changes to the constraints of the diel C₃ model were
486 required to capture the classical CAM cycle, the major change being to constrain
487 CO₂ exchange with the environment to zero during the light. This constraint forced
488 the model to carry out net carbon fixation during the night. Even though the model
489 was set up with free choices for the use of carboxylating enzymes and the nocturnal
490 carbon store (from malate, fumarate, citrate, starch and soluble sugars), the
491 conventional CAM cycle was predicted with PEP carboxylase as the carboxylating
492 enzyme and malate as the main temporary storage of fixed carbon in the dark. In
493 addition to malate, a small amount of citrate was predicted to accumulate during the
494 night, and this was used during the day in part to support nitrate assimilation and in
495 part for conversion to malate via isocitrate lyase. In fact, some CAM plants
496 accumulate a large amount of citrate during the night (Lüttge, 1988; Borland and
497 Griffiths, 1988) and it has been speculated that either ATP citrate lyase or the TCA
498 cycle are used for catabolism of this stored citrate ([Holtum et al., 2005](#)). ATP citrate
499 lyase produces oxaloacetate and acetyl-CoA from citrate, but since there is no major
500 sink for acetyl-CoA in the output constraints, this route was not chosen by the model.
501 One possible reason for preferring isocitrate lyase over the TCA cycle is that the
502 conversion of citrate to malate by the former route releases less CO₂ per molecule of
503 citrate (glyoxylate produced from isocitrate lyase is metabolised through the
504 photorespiratory pathway, producing 0.5 molecules of 3PGA and 0.5 molecules of
505 CO₂ per molecule of citrate catabolised) than the latter route (2 molecules of CO₂
506 released per molecule of citrate catabolised by aconitase, isocitrate dehydrogenase
507 and 2-oxoglutarate dehydrogenase). In the absence of measurements of ATP citrate
508 lyase and isocitrate lyase in CAM plants, it is not clear whether these two enzymes
509 are involved in the catabolism of citrate in vivo. Transcripts for both enzymes were
510 identified in a recent sequencing study of two agave species ([Gross et al., 2013](#)) but
511 at present, there is no quantitative data on the expression or activity levels that could
512 be used to discriminate between the possible routes. Ultimately, detailed metabolic
513 flux analysis would be required to examine this issue.

514

515 **Analysis of the energetics of CAM metabolism**

516

517 In the model of CAM leaf metabolism, where the model was free to choose
518 between different decarboxylating enzymes and storage compounds, malate
519 decarboxylation was predicted to be mainly carried out by PEPCK. This can be
520 explained by the observation that the mPEPCK-subtypes of CAM require fewer
521 photons, which leads to a lower total flux through the metabolic network (the
522 objective function that is optimised in the model) than the ME-subtypes (Fig. 7). In
523 other words, considering the whole network, the PEPCK-subtype is more
524 energetically efficient. This conclusion contrasts with previous manual calculations of
525 CAM-subtype energetics that considered the stoichiometry of a much smaller
526 metabolic network ([Winter and Smith, 1996](#)) and emphasises that the net balance of
527 ATP and NAD(P)H consumption is a property of the whole network.

528 While CAM undoubtedly represents an adaptation to arid conditions
529 ([Cushman, 2001](#); [Silvera et al., 2010](#)), the CAM cycle also acts as a CO₂-
530 concentrating mechanism and reduced CO₂ availability may have been the common,
531 original selection pressure that led to the evolution of CAM in both terrestrial and
532 aquatic environments ([Keeley and Rundel, 2003](#)). The CO₂ concentrating
533 mechanism may also suppress the carbon- and energy-consuming process of
534 photorespiration, although this is open to debate and depends critically upon the
535 internal CO₂:O₂ concentration ratio. However, there is a trade-off between the
536 energetic investment in the CO₂-concentrating mechanism in the form of the CAM
537 cycle and the benefit of suppressing photorespiration. The modelling results suggest
538 that the photon use of C₃ and CAM leaves are similar (Fig. 7), meaning that there is
539 little to be gained in terms of energetics in running the CAM cycle. However as well
540 as the running costs of the network, there is also the cost of the enzyme machinery.
541 A knock-on consequence of suppression of Rubisco oxygenase activity is that less
542 Rubisco protein is required to fix a given amount of carbon. Given that Rubisco
543 contributes up to 50% of the soluble proteins and 20-30% of the total nitrogen in a C₃
544 leaf ([Feller et al., 2008](#)), the predicted reduction of 22-32% of total Rubisco flux in
545 CAM compared to C₃ could be a significant benefit in terms of nitrogen use
546 efficiency. However, at the same time, there are additional enzyme machinery costs
547 for operating the CAM cycle. There are contradicting experimental observations
548 relating to nitrogen efficiency in CAM plants ([Luttge, 2004](#)). From the model

549 predictions, CAM requires 12-43% more total flux through the metabolic network
550 than C_3 . Although enzyme machinery cost per metabolic flux for each reaction will
551 vary depending on factors such as the size and the turnover rate of the enzyme, the
552 total network flux can be used as a proxy for the overall enzyme machinery cost by
553 averaging out the variation between reactions, although the extent to which this
554 assumption is distorted by very abundant enzymes with low K_{cat} values, such as
555 Rubisco, has not been tested. By balancing the benefit from reduced Rubisco
556 requirement with the increase in enzyme machinery costs in the rest of the metabolic
557 network, the total nitrogen invested in enzyme machinery is likely to be similar in C_3
558 and in CAM. Thus the modelling results suggest that energetics and nitrogen use
559 efficiency are unlikely to have been contributory drivers for the evolution of CAM
560 photosynthesis.

561

562 **CONCLUSION**

563

564 The diel FBA-modelling framework not only predicted known features of leaf
565 metabolism more accurately than a continuous light model, but it also allowed CAM
566 photosynthesis to be modelled at a network scale. This has allowed an accurate
567 accounting of the energetics of CAM metabolism, demonstrating that there are
568 unlikely to be substantial energetic benefits in CAM photosynthesis over C_3 , despite
569 the potential for suppression of photorespiration due to the CO_2 -concentrating effect
570 of the CAM cycle. In the current diel FBA framework it is assumed that the light and
571 dark phase each represent pseudo steady-states. This ignores known differences in
572 metabolic behaviour that occur within each phase, particularly at the light-dark
573 transition points, in both C_3 and CAM leaves. The framework can easily be extended
574 to account for such transitions, by further sub-dividing each phase. However, this
575 requires a more detailed knowledge of the input-output constraints at each time-step
576 and will lead to a more tightly constrained model where each time step is solved as
577 an independent or concatenated FBA problem. For this initial exploration, it was
578 preferable to apply minimal constraints to establish whether a metabolic network
579 optimised for efficiency (lowest overall flux) matched known configurations of C_3 and
580 CAM metabolism over a diel cycle.

581

582 **MATERIALS AND METHODS**

583

584 **Construction of a diel metabolic model**

585 The genome-scale metabolic model of Arabidopsis used for the analysis of
586 heterotrophic metabolism (Cheung et al., 2013) was adapted to model leaf
587 metabolism over a day-night cycle. The diel modelling framework was developed by
588 dividing the day-night cycle into two phases, light and dark, with metabolism in each
589 phase assumed to be at steady-state. The model was constructed by duplicating the
590 Arabidopsis genome-scale metabolic model, with the reactions and metabolites in
591 each duplicate labelled “_Light” or “_Dark” before the compartmentation suffix. In
592 addition, dummy reactions for “transporting” storage metabolites from one phase to
593 another were manually added with the suffix “_LightDark”. The diel model is
594 available in SBML format (Supplementary Data 1). Flux balance analysis and flux
595 variability analysis were implemented as before (Cheung et al., 2013).

596

597 **Quantitative comparison between flux ranges calculated from the diel model 598 and the continuous light model**

599

600 Flux ranges for reactions in the light were calculated using flux variability analysis for
601 the diel model, $(v_{min}^{diel}, v_{max}^{diel})$, and the continuous light model, $(v_{min}^{single}, v_{max}^{single})$.

602 Reversible reactions carrying fluxes in opposite directions in the two sets of flux
603 ranges were defined as reactions where either $v_{min}^{diel} \geq 0$ and $v_{max}^{single} \leq 0$ or $v_{min}^{single} \geq 0$
604 and $v_{max}^{diel} \leq 0$. Reactions with non-overlapping flux ranges were defined as reactions
605 where either $v_{min}^{diel} > v_{max}^{single}$ or $v_{min}^{single} > v_{max}^{diel}$. For reactions with non-overlapping flux
606 ranges that did not carry fluxes in opposite directions, a similarity measure was
607 calculated as $v_{max}^{low}/v_{min}^{high}$, where v_{max}^{low} is the maximum flux of the reaction with the
608 lower flux range of the pair and v_{min}^{high} is the minimum flux of the reaction with the
609 higher flux range. This measure varies from 0 to 1 where a value close to 0
610 represents a large difference between the flux ranges.

611

612 **Supplemental Data**

613

614 **Supplemental Table I.** Relative amino-acid composition in the phloem of
615 Arabidopsis.

616 **Supplemental Table II.** List of reactions with non-overlapping flux ranges between
617 the diel model and the single steady-state model and their similarity measures.

618 **Supplemental Table III.** Predicted fluxes for reactions in the light and the dark in a
619 leaf with either C3 or CAM photosynthesis.

620 **Supplemental Data 1.** Diel model of Arabidopsis leaf metabolism in SBML format.

621

622 **ACKNOWLEDGEMENTS**

623

624 We would like to thank Professor J.A.C. Smith (University of Oxford) for discussions
625 on the energetics of CAM metabolism.

626 **LITERATURE CITED**

627

628 **Antony E, Taybi T, Courbot M, Mugford ST, Smith JAC, Borland AM** (2008)
629 Cloning, localization and expression analysis of vacuolar sugar transporters in the
630 CAM plant *Ananas comosus* (pineapple). *J Exp Bot* **59**: 1895-1908

631

632 **Borland AM, Griffiths H** (1989) The regulation of citric acid accumulation and
633 carbon recycling during CAM in *Ananas comosus*. *J Exp Bot* **40**: 53-60

634

635 **Boyle NR, Morgan JA** (2009) Flux balance analysis of primary metabolism in
636 *Chlamydomonas reinhardtii*. *BMC Syst Biol* **3**: 4

637

638 **Cheung CYM, Williams TCR, Poolman MG, Fell DA, Ratcliffe RG, Sweetlove LJ**
639 (2013) A method for accounting for maintenance costs in flux balance analysis
640 improves the prediction of plant cell metabolic phenotypes under stress conditions.
641 *Plant J* **75**: 1050-1061

642

643 **Cushman JC** (2001) Crassulacean acid metabolism. A plastic photosynthetic
644 adaptation to arid environments. *Plant Physiol* **127**: 1439-1448

645

646 **Cushman JC, Tillett RL, Wood JA, Branco JM, Schlauch KA** (2008) Large-scale
647 mRNA expression profiling in the common ice plant, *Mesembryanthemum*

648 *crystallinum*, performing C₃ photosynthesis and Crassulacean acid metabolism
649 (CAM). J Exp Bot **59**: 1875-1894
650

651 **de Oliveira Dal'Molin CG, Quek LE, Palfreyman RW, Brumbley SM, Nielsen LK**
652 (2010a) AraGEM, a genome-scale reconstruction of the primary metabolic network in
653 Arabidopsis. Plant Physiol **152**: 579-589
654

655 **de Oliveira Dal'Molin CG, Quek LE, Palfreyman RW, Brumbley SM, Nielsen LK**
656 (2010b) C4GEM, a genome-scale metabolic model to study C₄ plant metabolism.
657 Plant Physiol **154**: 1871-1885
658

659 **de Oliveira Dal'Molin CG, Quek LE, Palfreyman RW, Nielsen LK** (2011) AlgaGEM
660 - a genome-scale metabolic reconstruction of algae based on the *Chlamydomonas*
661 *reinhardtii* genome. BMC Genomics **12 (Suppl 4)**: S5
662

663 **Delhon P, Gojon A, Tillard P, Passama L** (1995) Diurnal regulation of NO₃⁻ uptake
664 in soybean plants. 1. Changes in NO₃⁻ influx, efflux, and N utilization in the plant
665 during the day/night cycle. J Exp Bot **46**: 1585-1594
666

667 **Feller U, Anders I, Mae T** (2008) Rubiscolytics: fate of Rubisco after its enzymatic
668 function in a cell is terminated. J Exp Bot **59**: 1615-1624
669

670 **Gauthier PPG, Bligny R, Gout E, Mahé A, Nogués S, Hodges M, Tcherkez GGB**
671 (2010) *In folio* isotopic tracing demonstrates that nitrogen assimilation into glutamate
672 is mostly independent from current CO₂ assimilation in illuminated leaves of *Brassica*
673 *napus*. New Phytol **185**: 988-999
674

675 **Gibon Y, Bläsing OE, Palacios-Rojas N, Pankovic D, Hendriks JHM, Fisahn J,**
676 **Höhne M, Günther M, Stitt M** (2004) Adjustment of diurnal starch turnover to short
677 days: depletion of sugar during the night leads to a temporary inhibition of
678 carbohydrate utilization, accumulation of sugars and post-translational activation of
679 ADP-glucose pyrophosphorylase in the following light period. Plant J **39**: 847-862
680

681 **Gross SM, Martin JA, Simpson J, Abraham-Juarez MJ, Wang Z, Visel A** (2013)
682 *De novo* transcriptome assembly of drought tolerant CAM plants, *Agave deserti* and
683 *Agave tequilana*. BMC Genomics **14**: 563
684
685 **Gutteridge S, Pierce J** (2006) A unified theory for the basis of the limitations of the
686 primary reaction of photosynthetic CO₂ fixation: Was Dr. Pangloss right? Proc Natl
687 Acad Sci USA **103**: 7203-7204
688
689 **Hay J, Schwender J** (2011) Computational analysis of storage synthesis in
690 developing *Brassica napus* L. (oilseed rape) embryos: flux variability analysis in
691 relation to ¹³C metabolic flux analysis. Plant J **67**: 513-525
692
693 **Holtum JAM, Smith JAC, Neuhaus HE** (2005) Intracellular transport and pathways
694 of carbon flow in plants with crassulacean acid metabolism. Funct Plant Biol **32**: 429-
695 449
696
697 **Josse EM, Simkin AJ, Gaffe J, Laboure AM, Kuntz M, Carol P** (2000) A plastid
698 terminal oxidase associated with carotenoid desaturation during chromoplast
699 differentiation. Plant Physiol **123**: 1427-1436
700
701 **Keeley JE, Rundel PW** (2003) Evolution of CAM and C₄ carbon-concentrating
702 mechanisms. Int J Plant Sci **164**: S55-S77
703
704 **Knoop H, Gründel M, Zilliges Y, Lehmann R, Hoffmann S, Lockau W, Steuer R**
705 (2013) Flux balance analysis of cyanobacterial metabolism: the metabolic network of
706 *Synechocystis* sp. PCC 6803. PLoS Comput Biol **9**: e1003081
707
708 **Knoop H, Zilliges Y, Lockau W, Steuer R** (2010) The metabolic network of
709 *Synechocystis* sp. PCC 6803: systemic properties of autotrophic growth. Plant
710 Physiol **154**: 410-422
711
712 **Kramer DM, Evans JR** (2011) The importance of energy balance in improving
713 photosynthetic productivity. Plant Physiol **155**: 70-78
714

715 **Lüttge U** (1988) Day-night changes of citric-acid levels in crassulacean acid
716 metabolism: phenomenon and ecophysiological significance. *Plant Cell Environ* **11**:
717 445-451
718

719 **Lüttge U** (2004) Ecophysiology of crassulacean acid metabolism (CAM). *Ann Bot*
720 **93**: 629-652
721

722 **Lüttge U** (2011) Photorespiration in phase III of crassulacean acid metabolism:
723 evolutionary and ecophysiological implications. *Prog Bot* **72**: 371-384
724

725 **Macduff JH, Bakken AK** (2003) Diurnal variation in uptake and xylem contents of
726 inorganic and assimilated N under continuous and interrupted N supply to *Phleum*
727 *pratense* and *Festuca pratensis*. *J Exp Bot* **54**: 431-444
728

729 **Maurino VG, Weber AP** (2013) Engineering photosynthesis in plants and synthetic
730 microorganisms. *J Exp Bot* **64**: 743-751
731

732 **McRae SR, Christopher JT, Smith JAC, Holtum JAM** (2002) Sucrose transport
733 across the vacuolar membrane of *Ananas comosus*. *Funct Plant Biol* **29**: 717-724
734

735 **Montagud A, Navarro E, Fernandez de Cordoba P, Urchueguia JF, Patil KR**
736 (2010) Reconstruction and analysis of genome-scale metabolic model of a
737 photosynthetic bacterium. *BMC Syst Biol* **4**: 156
738

739 **Neuhaus HE, Schulte N** (1996) Starch degradation in chloroplasts isolated from C₃
740 or CAM (crassulacean acid metabolism)-induced *Mesembryanthemum crystallinum*
741 L.. *Biochem J* **318**: 945-953
742

743 **Nguyen-Quoc B, Krivitzky M, Huber SC, Lecharyn A** (1990) Sucrose synthase in
744 developing maize leaves: regulation of activity by protein level during the import to
745 export transition. *Plant Physiol* **94**: 516-523
746

747 **Niewiadomski P, Knappe S, Geimer S, Fischer K, Schulz B, Unte US, Rosso**
748 **MG, Ache P, Flügge UI, Schneider A** (2005) The Arabidopsis plastidic glucose 6-

749 phosphate/phosphate translocator GPT1 is essential for pollen maturation and
750 embryo sac development. *Plant Cell* **17**: 760-775
751

752 **Nogales J, Gudmundsson S, Knight EM, Palsson BO, Thiele I** (2012) Detailing
753 the optimality of photosynthesis in cyanobacteria through systems biology analysis.
754 *Proc Natl Acad Sci USA* **109**: 2678-2683
755

756 **Poolman MG, Kundu S, Shaw R, Fell DA** (2013) Responses to light intensity in a
757 genome-scale model of rice metabolism. *Plant Physiol* **162**: 1060-1072
758

759 **Saha R, Suthers P, Maranas C** (2011) *Zea mays* i RS1563: a comprehensive
760 genome-scale metabolic reconstruction of maize metabolism. *PloS ONE* **6**: e21784
761

762 **Saha R, Verseput AT, Berla BM, Mueller TJ, Pakrasi HB, Maranas CD** (2012)
763 Reconstruction and comparison of the metabolic potential of cyanobacteria
764 *Cyanothece* sp. ATCC 51142 and *Synechocystis* sp. PCC 6803. *PLoS ONE* **7**:
765 e48285
766

767 **Scheible WR, Krapp A, Stitt M** (2000) Reciprocal diurnal changes of
768 phosphoenolpyruvate carboxylase expression and cytosolic pyruvate kinase, citrate
769 synthase and NADP-isocitrate dehydrogenase expression regulate organic acid
770 metabolism during nitrate assimilation in tobacco leaves. *Plant Cell Environ* **23**:
771 1155-1167
772

773 **Siebrecht S, Herdel K, Schurr U, Tischner R** (2003) Nutrient translocation in the
774 xylem of poplar - diurnal variations and spatial distribution along the shoot axis.
775 *Planta* **217**: 783-793
776

777 **Silvera K, Neubig KM, Whitten WM, Williams NH, Winter K, Cushman JC** (2010)
778 Evolution along the crassulacean acid metabolism continuum. *Funct Plant Biol* **37**:
779 995-1010
780

781 **Smith JAC, Bryce JH** (1992) Metabolite compartmentation and transport in CAM
782 plants. In AK Tobin, ed, Plant organelles. Cambridge University Press, Cambridge,
783 pp 141-167
784

785 **Stitt M, Muller C, Matt P, Gibon Y, Carillo P, Morcuende R, Scheible WR, Krapp**
786 **A** (2002) Steps towards an integrated view of nitrogen metabolism. J Exp Bot **53**:
787 959-970
788

789 **Sweetlove LJ, Beard KFM, Nunes-Nesi A, Fernie AR, Ratcliffe RG** (2010) Not
790 just a circle: flux modes in the plant TCA cycle. Trends Plant Sci **15**: 462-470
791

792 **Sweetlove LJ, Ratcliffe RG** (2011) Flux-balance modelling of plant metabolism.
793 Front Plant Sci **2**: 38
794

795 **Szecowka M, Heise R, Tohge T, Nunes-Nesi A, Vosloh D, Huege J, Feil R, Lunn**
796 **J, Nikoloski Z, Stitt M, Fernie AR, Arrivault S** (2013) Metabolic fluxes in an
797 illuminated Arabidopsis rosette. Plant Cell **25**: 694-714
798

799 **Tcherkez G, Mahe A, Gauthier P, Mauve C, Gout E, Bligny R, Cornic G, Hodges**
800 **M** (2009) *In folio* respiratory fluxomics revealed by ¹³C isotopic labeling and H/D
801 isotope effects highlight the noncyclic nature of the tricarboxylic acid "cycle" in
802 illuminated leaves. Plant Physiol **151**: 620-630
803

804 **Tovar-Mendez A, Miernyk JA, Randall DD** (2003) Regulation of pyruvate
805 dehydrogenase complex activity in plant cells. Eur J Biochem **270**: 1043-1049
806

807 **Weise SE, van Wijk KJ, Sharkey TD** (2011) The role of transitory starch in C₃,
808 CAM, and C₄ metabolism and opportunities for engineering leaf starch accumulation.
809 J Exp Bot **62**: 3109-3118
810

811 **Wilkinson TL, Douglas AE** (2003) Phloem amino acids and the host plant range of
812 the polyphagous aphid, *Aphis fabae*. Entomol Exp Appl **106**: 103-113
813

814 **Winter K, Smith JACS** (1996) Crassulacean acid metabolism: current status and
815 perspectives. In K Winter, JACS Smith, eds, Crassulacean acid metabolism.
816 Biochemistry, ecophysiology and evolution. Springer-Verlag, Berlin, pp 389-426

817

818 **Yamamoto H, Peng LW, Fukao Y, Shikanai T** (2011) An Src homology 3 domain-
819 like fold protein forms a ferredoxin binding site for the chloroplast NADH
820 dehydrogenase-like complex in *Arabidopsis*. Plant Cell **23**: 1480-1493

821

822 **Yan XY, Tan DKY, Inderwildi OR, Smith JAC, King DA** (2011) Life cycle energy
823 and greenhouse gas analysis for agave-derived bioethanol. Energy Environ Sci **4**:
824 3110-3121

825

826 **Zeeman SC, Smith SM, Smith AM** (2004) The breakdown of starch in leaves.
827 NewPhytol **163**: 247-261

828

829 **FIGURE LEGENDS**

830

831 **Figure 1.** Flux-balance framework for integrated metabolic modelling of the day and
832 night phases of a mature leaf. The light dark phases are represented by the white
833 and grey backgrounds of the diagram respectively. Metabolites shown in the dashed
834 rectangles between the two phases represent potential storage compounds. Starch,
835 glucose, fructose, malate, fumarate, citrate and nitrate were allowed to accumulate in
836 the light and in the dark as denoted by the arrows pointing towards the light and dark
837 states. Twenty common amino-acids were allowed to accumulate in the light but not
838 in the dark as denoted by the arrow pointing from the light phase to the dark phase.
839 Export to the phloem was set to four sucrose to one amino-acid, with 18 different
840 amino-acids in the proportions shown in Supplemental Table 1. The export rate was
841 set to be three times greater in the light than in the dark. Nitrate was set as the sole
842 nitrogen source with the ratio of nitrate uptake from the phloem in the light to that in
843 the dark set to 3 to 2. Cellular maintenance costs in the dark were set to a fixed
844 value where the carbon exported during the night roughly equalled the carbon
845 released as CO₂ in the dark phase. Maintenance costs were assumed to be the
846 same in the light and the dark. The ratio of ATP maintenance cost to NADPH
847 maintenance cost was set to 3 to 1.

848

849 **Figure 2.** Metabolic routes for glutamate biosynthesis from two modelling
850 approaches. A single steady-state model in constant light is shown on the left and
851 the diel modelling framework on the right. In constant light, the carbon skeletons for
852 glutamine synthesis were predicted to be supplied via a metabolic route in which
853 threonine is metabolised in the cytosol to acetate, transported to the peroxisome and
854 metabolised to citrate which is exported to the cytosol and converted to 2-
855 oxoglutarate. Using the diel modelling framework, the model predicted the use of
856 citrate stored in the dark to provide the carbon skeletons for glutamate synthesis in
857 the light. Abbreviations: PEP, phospho*en*o/pyruvate; OAA oxaloacetate. The
858 thickness of the arrows is scaled to indicate relative flux magnitudes (in molar units).

859

860 **Figure 3.** Predicted flux map of metabolism for a mature C₃ leaf over a day-night
861 cycle. The light dark phases are represented by the white grey backgrounds
862 respectively. Metabolites shown in the dashed rectangles between the two phases

863 represent storage compounds. The thickness of the arrows is proportional to the
864 metabolic flux through the reactions (in molar units). Metabolic processes listed
865 within rounded rectangles carry fluxes too large to be represented on the flux map.
866 Abbreviations: ETC, electron transport chain; OPPP, oxidative pentose phosphate
867 pathway; TCA, tricarboxylic acid.

868

869 **Figure 4.** Flux predictions through the TCA cycle and pyruvate dehydrogenase in a
870 C₃ leaf in the light and the dark. A non-cyclic mode with two separate branches,
871 citrate to 2-oxoglutarate and oxaloacetate and fumarate to malate, was predicted to
872 operate in the light. A cyclic mode of the TCA cycle was predicted to operate in the
873 dark, mainly to produce ATP via oxidative phosphorylation. Fluxes illustrated are net
874 conversion between metabolites over all subcellular compartments. The thickness of
875 the arrows is proportional to the metabolic fluxes through the reactions (in molar
876 units). Citrate stored in the dark is represented by an arrow pointing from the dark
877 phase to the light phase. Malate storage is not illustrated in this diagram.

878

879 **Figure 5.** Reductant shuttling between subcellular compartments and the production
880 and consumption of NADH in mitochondria in the light. Left-pointing arrows represent
881 reductant-consuming reactions; right-pointing arrows represent reductant-producing
882 reactions. The thickness of the solid arrows is proportional to the metabolic flux
883 through the reactions (in molar units), except for the conversion between 3PGA and
884 GAP in the chloroplast where the zig-zag line across the arrow indicates that the flux
885 is too large to be illustrated to scale in the diagram. Reductant shuttles between four
886 subcellular compartments, cytosol, chloroplast, mitochondria and peroxisome, are
887 shown with dashed arrows representing transfer of metabolites between
888 compartments. Abbreviations: 2OG, 2-oxoglutarate; 3PGA, 3-phosphoglycerate;
889 ETC, electron transport chain; GAP, glyceraldehyde 3-phosphate; OAA,
890 oxaloacetate.

891

892 **Figure 6.** Flux predictions through the TCA cycle and related reactions in a CAM
893 leaf. A non-cyclic mode with two distinct branches, citrate to 2-oxoglutarate and
894 succinate to oxaloacetate, was predicted to operate in the light. The two branches of
895 the TCA cycle are connected by isocitrate lyase which converts isocitrate into
896 succinate and glyoxylate. A cyclic mode of the TCA cycle was predicted to operate in

897 the dark, mainly to contribute to ATP production via oxidative phosphorylation.
898 Fluxes illustrated are net conversion between metabolites over all subcellular
899 compartments. The thickness of the arrows is proportional to the metabolic flux
900 through the reactions (in molar units), except for the conversion between malate and
901 oxaloacetate where the zig-zag line across the arrow indicates that the flux is too
902 large to be illustrated to scale in the diagram. Citrate stored in the dark is
903 represented by an arrow pointing from the dark phase to the light phase. Malate
904 storage is not illustrated in this diagram.

905

906 **Figure 7.** Comparison of model predictions between C_3 and the various subtypes of
907 CAM defined in Table II. The model predictions for photon use, Rubisco carboxylase
908 flux, Rubisco oxygenase flux, total flux through Rubisco and the total flux in the
909 metabolic model are shown with values scaled as a percentage of the value in the
910 C_3 leaf model.

911

912 **Table I.** List of reactions in the light that have different fluxes in the diel model and
 913 the continuous light model

914 Reactions with similarity measures less than 0.25 are listed, where a small
 915 value represents a large difference in fluxes from the two modelling approaches (see
 916 Supplemental Table II for a complete list of reactions with non-overlapping flux
 917 ranges). The metabolic context of the reactions is listed in the column on the right.

Reaction name	Similarity Measure	Metabolic context
Reactions with higher flux in the diel model		
Plastidic ADPglucose pyrophosphorylase	0	Starch synthesis
Plastidic starch synthase	0	Starch synthesis
Plastidic phosphoglucose isomerase	0	Starch synthesis
Plastidic phosphoglucomutase	0	Starch synthesis
Tonoplast citrate/H ⁺ antiporter	0	Storage in the vacuole
Tonoplast malate/H ⁺ antiporter	0	Storage in the vacuole
Tonoplast fumarate/H ⁺ antiporter	0	Storage in the vacuole
Tonoplast nitrate transporter	0	Storage in the vacuole
Tonoplast PP _i ase	0	Storage in the vacuole
Plastidic alkaline pyrophosphatase	0.015	Related to starch synthesis
Reactions with higher flux in the continuous-light model		
Peroxisomal inorganic pyrophosphatase	0	Related to Glu and Gln synthesis
Peroxisomal phosphate transporter	0	Related to Glu and Gln synthesis
Peroxisomal citrate synthase	0	Related to Glu and Gln synthesis
Peroxisomal acetyl-CoA synthetase	0	Related to Glu and Gln synthesis
Peroxisomal AMP/ATP antiporter	0	Related to Glu and Gln synthesis
Peroxisomal acetate transporter	0	Related to Glu and Gln synthesis
Peroxisomal citrate transporter	0	Related to Glu and Gln synthesis
Cytosolic threonine aldolase	0.019	Related to Glu and Gln synthesis
Cytosolic aldehyde dehydrogenase	0.019	Related to Glu and Gln synthesis
Plastidic ATP/ADP antiporter	0.093	Export of ATP from the chloroplast
Plastidic threonine transporter	0.123	Related to Glu and Gln synthesis
Plastidic threonine synthase	0.145	Related to Glu and Gln synthesis
Plastidic homoserine kinase	0.153	Related to Glu and Gln synthesis
Plastidic homoserine dehydrogenase	0.161	Related to Glu and Gln synthesis
Plastidic aspartate kinase	0.180	Related to Glu and Gln synthesis
Plastidic aspartate semialdehyde dehydrogenase	0.180	Related to Glu and Gln synthesis
Mitochondrial ATP/AMP antiporter	0.202	Related to Glu and Gln synthesis
Mitochondrial adenylate kinase	0.202	Related to Glu and Gln synthesis
Plastidic aspartate transporter	0.208	Related to Glu and Gln synthesis

918 **Table II.** Constraints applied for modelling leaf metabolism in C₃ and various
 919 subtypes of CAM

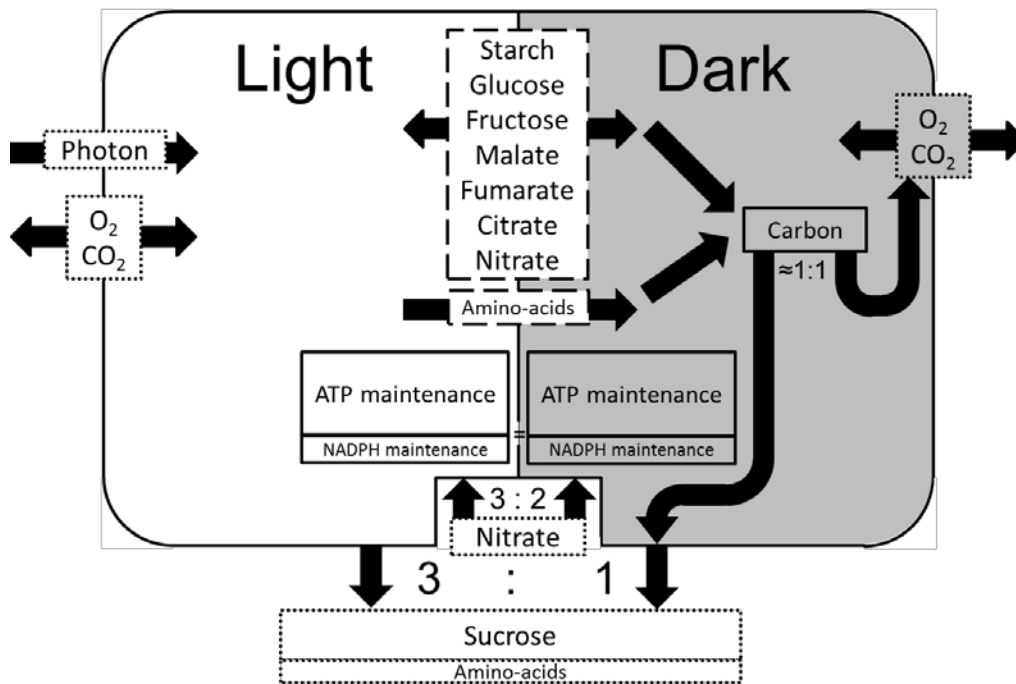
920

Constraints for different modes of photosynthesis		C ₃	CAM				
			generic	starch-PEPCK	starch-ME	sugars-PEPCK	sugars-ME
CO ₂ exchange	CO ₂ exchange in light	Free	0				
Photorespiration	Rubisco CO ₂ :O ₂	3:1	Unconstrained in light, 3:1 in dark				
Transporter	chloroplast G6P-Pi	0	Free				

Metabolic reactions	PEPCK	Free	Free	Free	0	Free	0
	ME	Free	Free	0	Free	0	Free
	pyruvate, P _i dikinase	Free	Free	0	Free	0	Free
Storage compounds	Starch	Free	Free	Free	Free	0	0
	Soluble sugars	Free	Free	0	0	Free	Free

921

922

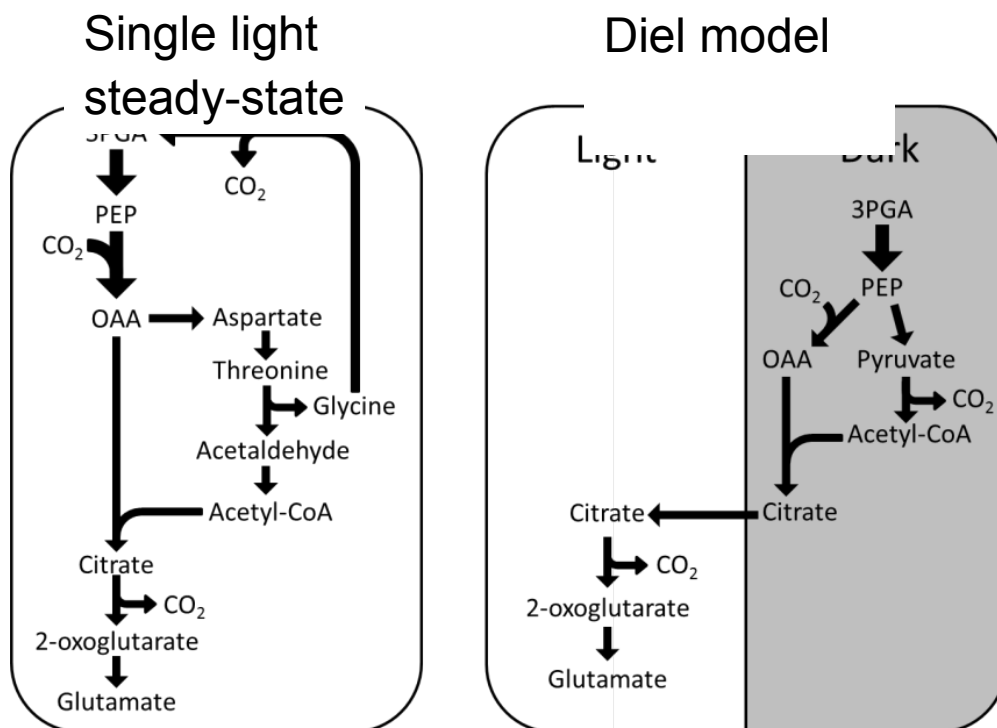


923

924

925 **Figure 1.** Flux-balance framework for integrated metabolic modelling of the day and
 926 night phases of a mature leaf. The light dark phases are represented by the white
 927 and grey backgrounds of the diagram respectively. Metabolites shown in the dashed
 928 rectangles between the two phases represent potential storage compounds. Starch,
 929 glucose, fructose, malate, fumarate, citrate and nitrate were allowed to accumulate in
 930 the light and in the dark as denoted by the arrows pointing towards the light and dark
 931 states. Twenty common amino-acids were allowed to accumulate in the light but not
 932 in the dark as denoted by the arrow pointing from the light phase to the dark phase.
 933 Export to the phloem was set to four sucrose to one amino-acid, with 18 different
 934 amino-acids in the proportions shown in Supplemental Table 1. The export rate was
 935 set to be three times greater in the light than in the dark. Nitrate was set as the sole
 936 nitrogen source with the ratio of nitrate uptake from the phloem in the light to that in
 937 the dark set to 3 to 2. Cellular maintenance costs in the dark were set to a fixed
 938 value where the carbon exported during the night roughly equalled the carbon
 939 released as CO₂ in the dark phase. Maintenance costs were assumed to be the
 940 same in the light and the dark. The ratio of ATP maintenance cost to NADPH
 941 maintenance cost was set to 3 to 1.

942

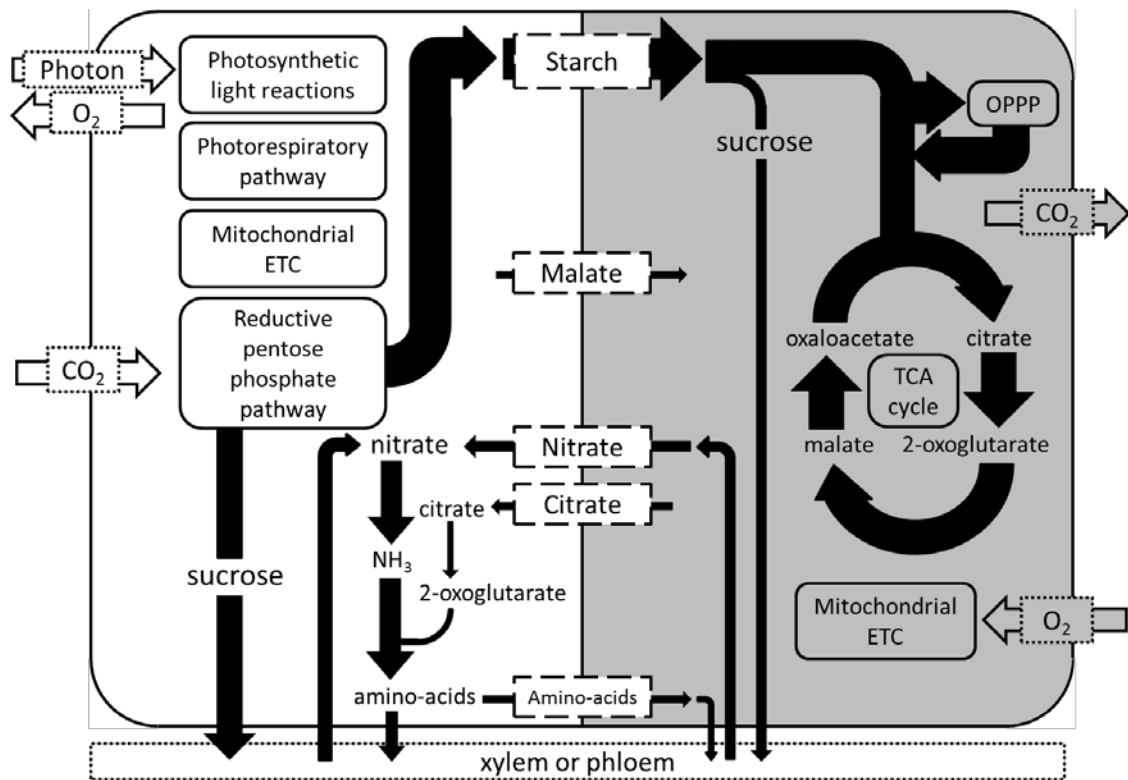


943

944

945

946 **Figure 2.** Metabolic routes for glutamate biosynthesis from two modelling
 947 approaches. A single steady-state model in constant light is shown on the left and
 948 the diel modelling framework on the right. In constant light, the carbon skeletons for
 949 glutamine synthesis were predicted to be supplied via a metabolic route in which
 950 threonine is metabolised in the cytosol to acetate, transported to the peroxisome and
 951 metabolised to citrate which is exported to the cytosol and converted to 2-
 952 oxoglutarate. Using the diel modelling framework, the model predicted the use of
 953 citrate stored in the dark to provide the carbon skeletons for glutamate synthesis in
 954 the light. Abbreviations: PEP, phospho*en*o/pyruvate; OAA oxaloacetate. The
 955 thickness of the arrows is scaled to indicate relative flux magnitudes (in molar units).
 956



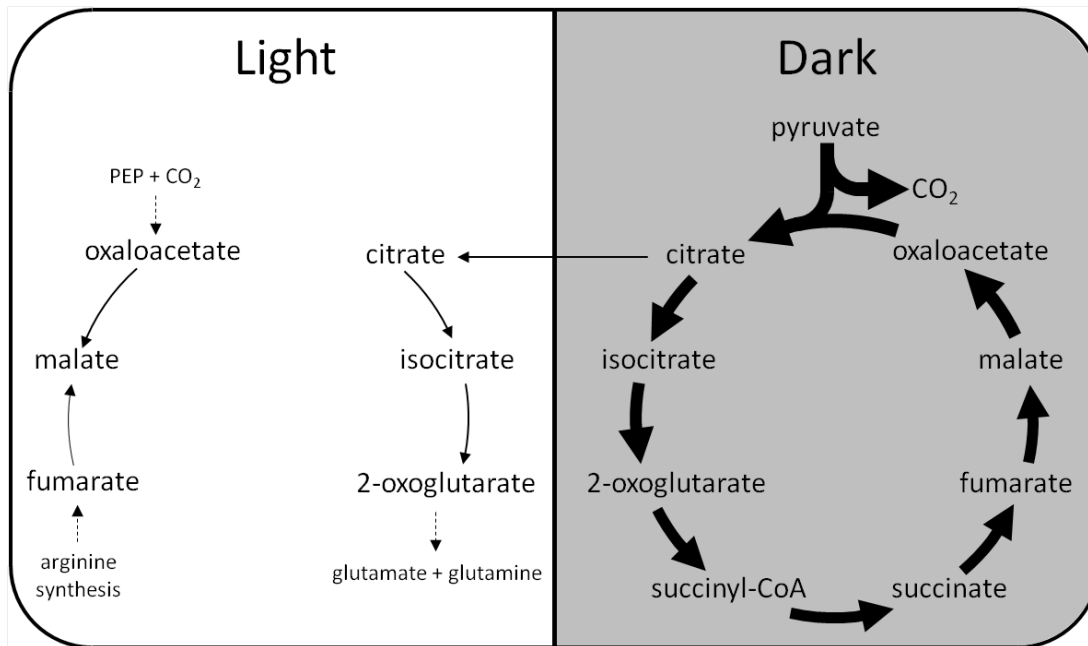
957

958

959

960 **Figure 3.** Predicted flux map of metabolism for a mature C_3 leaf over a day-night
 961 cycle. The light dark phases are represented by the white grey backgrounds
 962 respectively. Metabolites shown in the dashed rectangles between the two phases
 963 represent storage compounds. The thickness of the arrows is proportional to the
 964 metabolic flux through the reactions (in molar units). Metabolic processes listed
 965 within rounded rectangles carry fluxes too large to be represented on the flux map.
 966 Abbreviations: ETC, electron transport chain; OPPP, oxidative pentose phosphate
 967 pathway; TCA, tricarboxylic acid.

968

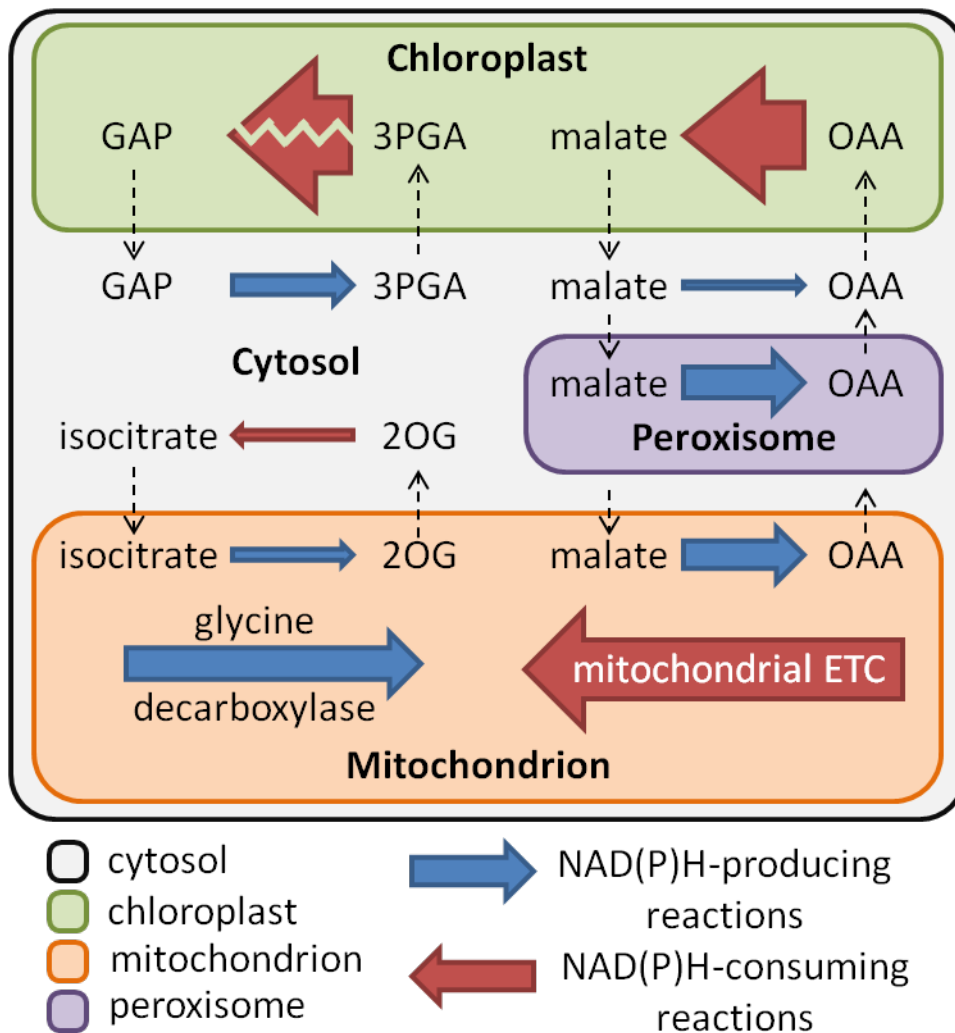


970

971

972

973 **Figure 4.** Flux predictions through the TCA cycle and pyruvate dehydrogenase in a
 974 C₃ leaf in the light and the dark. A non-cyclic mode with two separate branches,
 975 citrate to 2-oxoglutarate and oxaloacetate and fumarate to malate, was predicted to
 976 operate in the light. A cyclic mode of the TCA cycle was predicted to operate in the
 977 dark, mainly to produce ATP via oxidative phosphorylation. Fluxes illustrated are net
 978 conversion between metabolites over all subcellular compartments. The thickness of
 979 the arrows is proportional to the metabolic fluxes through the reactions (in molar
 980 units). Citrate stored in the dark is represented by an arrow pointing from the dark
 981 phase to the light phase. Malate storage is not illustrated in this diagram.

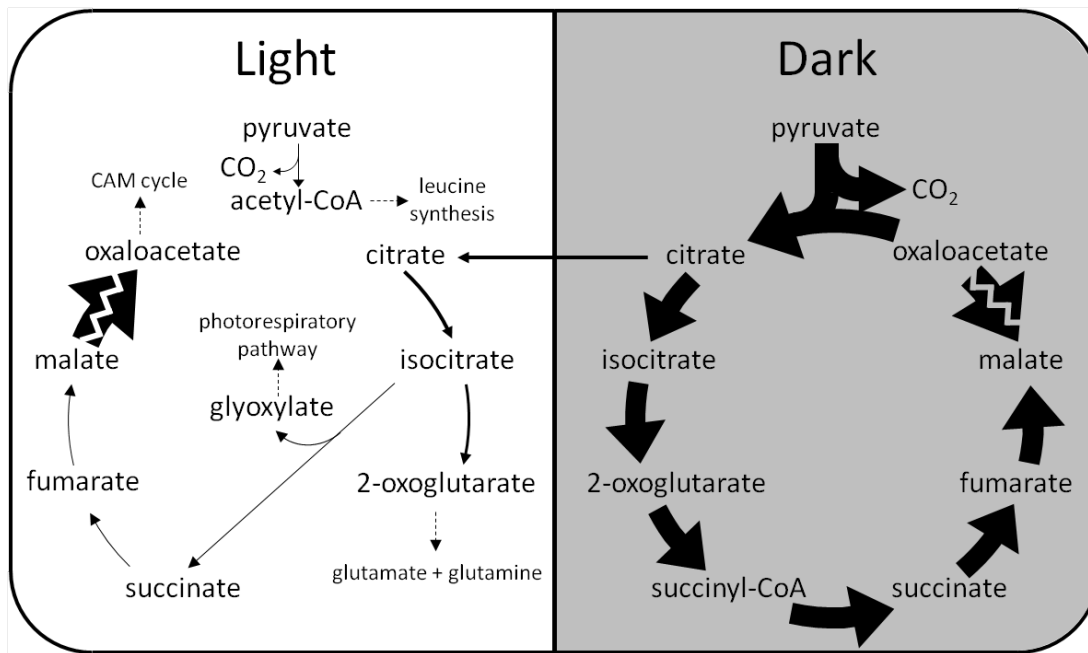


982

983

984

985 **Figure 5.** Reductant shuttling between subcellular compartments and the production
 986 and consumption of NADH in mitochondria in the light. Left-pointing arrows represent
 987 reductant-consuming reactions; right-pointing arrows represent reductant-producing
 988 reactions. The thickness of the solid arrows is proportional to the metabolic flux
 989 through the reactions (in molar units), except for the conversion between 3PGA and
 990 GAP in the chloroplast where the zig-zag line across the arrow indicates that the flux
 991 is too large to be illustrated to scale in the diagram. Reductant shuttles between four
 992 subcellular compartments, cytosol, chloroplast, mitochondria and peroxisome, are
 993 shown with dashed arrows representing transfer of metabolites between
 994 compartments. Abbreviations: 2OG, 2-oxoglutarate; 3PGA, 3-phosphoglycerate;
 995 ETC, electron transport chain; GAP, glyceraldehyde 3-phosphate; OAA,
 996 oxaloacetate.



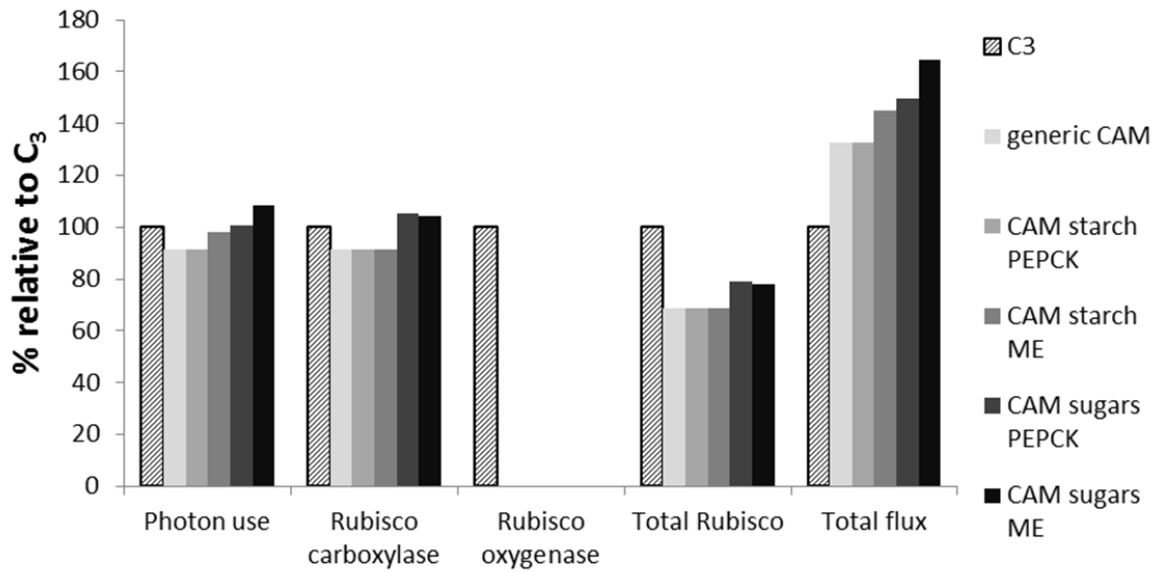
998

999

1000

1001 **Figure 6.** Flux predictions through the TCA cycle and related reactions in a CAM
 1002 leaf. A non-cyclic mode with two distinct branches, citrate to 2-oxoglutarate and
 1003 succinate to oxaloacetate, was predicted to operate in the light. The two branches of
 1004 the TCA cycle are connected by isocitrate lyase which converts isocitrate into
 1005 succinate and glyoxylate. A cyclic mode of the TCA cycle was predicted to operate in
 1006 the dark, mainly to contribute to ATP production via oxidative phosphorylation.
 1007 Fluxes illustrated are net conversion between metabolites over all subcellular
 1008 compartments. The thickness of the arrows is proportional to the metabolic flux
 1009 through the reactions (in molar units), except for the conversion between malate and
 1010 oxaloacetate where the zig-zag line across the arrow indicates that the flux is too
 1011 large to be illustrated to scale in the diagram. Citrate stored in the dark is
 1012 represented by an arrow pointing from the dark phase to the light phase. Malate
 1013 storage is not illustrated in this diagram.

1014



1015

1016

1017

1018 **Figure 7.** Comparison of model predictions between C₃ and the various subtypes of
 1019 CAM defined in Table II. The model predictions for photon use, Rubisco carboxylase
 1020 flux, Rubisco oxygenase flux, total flux through Rubisco and the total flux in the
 1021 metabolic model are shown with values scaled as a percentage of the value in the
 1022 C₃ leaf model.

1023

1024